UNIVERSITY OF BIRMINGHAM

University of Birmingham
Research at Birmingham

Topology-based fluorescence image analysis for automated cell identification and segmentation

Panconi, Luca; Makarova, Maria; Lambert, Eleanor; May, Robin; Owen, Dylan

Document Version
Publisher's PDF, also known as Version of record

[Link to publication on Research at Birmingham portal](#)

JOURNAL OF
BIOPHOTONICS

Topology-based fluorescence image analysis for automated cell identification and segmentation

Luca Panconi[1] | **Maria Makarova**[2] | **Eleanor R. Lambert**[1] | **Robin C. May**[3] | **Dylan M. Owen**[1]

[1]Institute of Immunology and Immunotherapy, School of Mathematics and Centre of Membrane Proteins and Receptors, University of Birmingham, Birmingham, UK

[2]Institute of Metabolism and Systems Research, University of Birmingham, Birmingham, UK

[3]School of Biosciences and Institute of Microbiology and Infection, University of Birmingham, Birmingham, UK

Correspondence
Luca Panconi, Institute of Immunology and Immunotherapy, School of Mathematics and Centre of Membrane Proteins and Receptors, University of Birmingham, Birmingham, UK.
Email: lxp609@student.bham.ac.uk

Abstract

Cell segmentation refers to the body of techniques used to identify cells in images and extract biologically relevant information from them; however, manual segmentation is laborious and subjective. We present Topological Boundary Line Estimation using Recurrence Of Neighbouring Emissions (TOBLERONE), a topological image analysis tool which identifies persistent homological image features as opposed to the geometric analysis commonly employed. We demonstrate that topological data analysis can provide accurate segmentation of arbitrarily-shaped cells, offering a means for automatic and objective data extraction. One cellular feature of particular interest in biology is the plasma membrane, which has been shown to present varying degrees of lipid packing, or membrane order, depending on the function and morphology of the cell type. With the use of environmentally-sensitive dyes, images derived from confocal microscopy can be used to quantify the degree of membrane order. We demonstrate that TOBLERONE is capable of automating this task.

KEYWORDS
biology, confocal microscopy, data analysis, dyes, lipid, plasma membrane
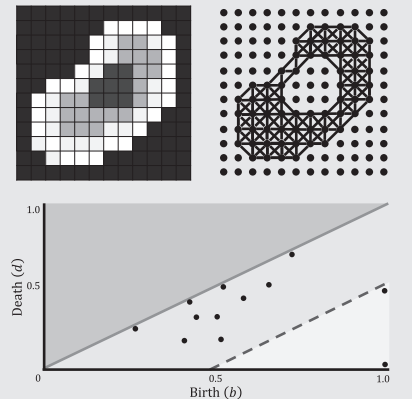
1 | INTRODUCTION

Fluorescence microscopy is fundamental to modern cell biology [1]. However, in order to extract biologically relevant information from acquired images, researchers are required to first identify the regions of the image corresponding to individual cells or their enclosed organelles. The introduction of cell segmentation techniques allows for automated partitioning of images derived from fluorescence microscopy. In general, these techniques can be classified into machine learning-based methods and non-machine learning-based methods. Both variants present a range of drawbacks.

Non-machine learning methods typically require images with individual components of the cell stained specifically so that the algorithm can detect them [2]. They are usually dependent on cell geometry (in particular, convexity), making them incapable of identifying cells or organelles with particularly complex structures [3]. Additionally, they often require additional steps such as image reconstruction or seed-point extraction and typically have low generalisability for new applications [4, 5].

Machine learning-based methods employ a range of data manipulation techniques which learn from training data to make informed predictions on new images. In image analysis, these techniques are typically limited to supervised learning and therefore inherently require training data, using large sets of existing images which have already undergone cell segmentation [6]. Training data must typically be derived manually, which is a time-consuming process and creates subjectivity in the results. At the extremity of supervised object classification is deep learning. These methods carry several disadvantages in that they require training data to return accurate results and have a range of possible input parameters and settings (eg, network architecture and training hyperparameters) [1, 7, 8]. Even with the advantages they bring, machine learning methods may also be limited to particular cell geometries [9].

In this work, we devise an image analysis algorithm for efficient cell and organelle segmentation irrespective of morphological and geometric distinctions. TOpological Boundary Line Estimation using Recurrence Of Neighbouring Emissions (TOBLERONE) enables identification of intensity modes within images by means of the topological data analysis techniques known as persistent homology and mode seeking. Topological image analysis is itself a relatively young field, which has shown promise in probing microbiology [10]. Similar algorithms have used this form of analysis to segment nuclei in histological slides of liver tissue [11]. Here, we have adapted this concept to identify any biological structure in fluorescence images.

Persistent homology was initially developed to study qualitative features of data sets [12], and then as a prerequisite for cluster analysis, with filtrations constructed over a point cloud in which each localisation is assigned a local density given by the number of neighbouring points in a specified search radius [13]. In this instance, filtrations are constructed over a field of pixels with the "local density" derived exclusively from the fluorescence intensity of the underlying image.

Here, we compare the sensitivity and specificity of TOBLERONE to existing image segmentation methods on simulated data under varying degrees of noise and blur. Then, to demonstrate the method on experimental, biological data we show that TOBLERONE can segment pixels corresponding to the plasma membrane of pan-membrane-stained cells. There is evidence that plasma membranes can comprise an extensive range of lipid packing states with varying levels of molecular order [14, 15]. It has been shown that such lipid packing states may be specifically regulated by cells during active cellular processes, suggesting that lipid-mediated membrane organisation has functional consequences [16, 17]. Using environmentally-sensitive membrane probes, we highlight the efficacy of TOBLERONE in mapping heterogeneity of lipid packing across the plasma membrane of the pathogenic yeast species, *Cryptococcus gattii*, and in mammalian cells.

2 | MATERIALS AND METHODS

HEK293 cells were cultured in DMEM supplemented with 10% FCS at 37°C in a 5% CO_2 incubator. Cells were split and seeded into an 8-well coverslip bottomed Ibidi microscope chamber 24 hours prior to imaging. They were then stained with either di-4-ANEPPDHQ (5 μM) from an ethanol (5 mM) stock solution (to stain membranes) or 1× Nucblue (to stain DNA) 30 minutes prior to imaging. *C gattii* cells were cultured in yeast-peptone-dextrose (YPD) broth at 25°C with rotation and stained with di-4-ANEPPDHQ in the same way. Treatment with a hydroxyoleic acid (100 μM) and 7-ketocholesterol (20 μM) was performed 3 hours before imaging and staining.

Live HEK293 and *C gattii* cells were imaged on a Zeiss 780 laser-scanning confocal microscope at 37°C. For di-4-ANEPPDHQ, 488 nm excitation was used with fluorescence collected in two wavelength ranges: 500-580 nm and 620-750 nm. GP values from these two images were calculated as previously described [15]. For Nucblue, excitation was at 405 nm with fluorescence collected in the range 420-500 nm. In both cases, 4× line averaging was used.

The TOBLERONE software package v1.0.0 was written in the R programming language v4.2.0, and employed in the integrated development environment RStudio, version 2022.07.1 + 554. The code incorporated the tiff library for image manipulation and the built-in grid package for display. TOBLERONE is available for use under GNU General Public License v3.0, see Appendix S1 for code. Otsu thresholding and the Watershed algorithm were both undertaken using built-in functions with the EBImage R package v4.19.13 [18]. Otsu thresholding is inherently parameterless so required no finetuning. Appropriate input parameters were determined iteratively for the watershed algorithm.

Simulated 8-bit images were generated by manually drawing arbitrary shapes in GIMP raster graphics editor.
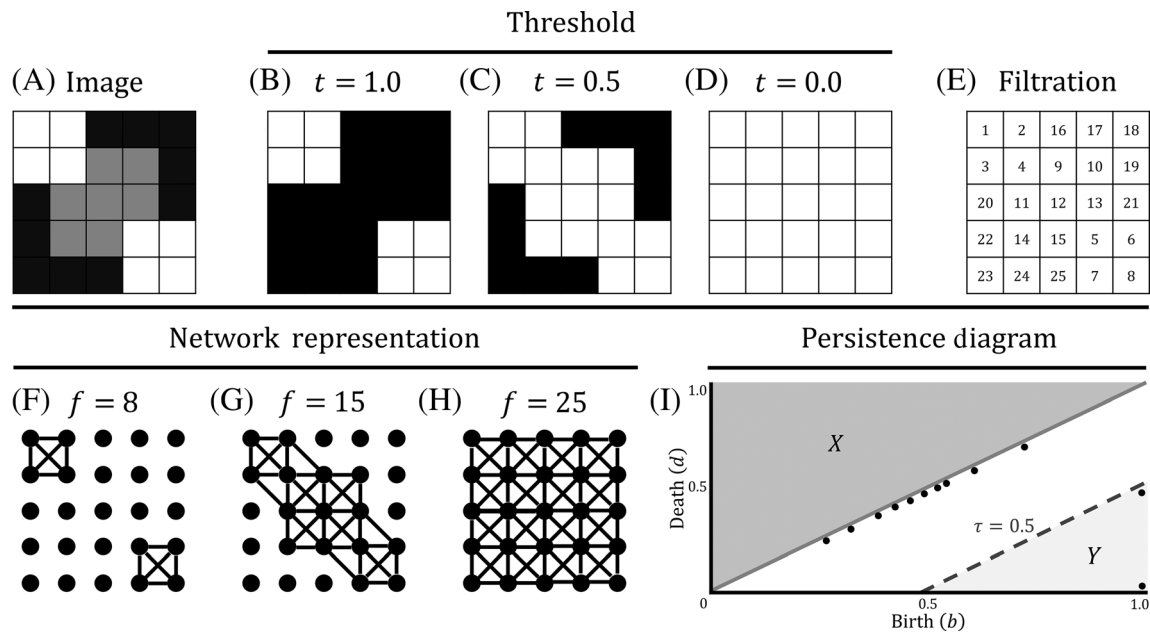
FIGURE 1 A, A schematic image with 25 pixels, represented by a matrix in which each entry contains a numeric value between 0 and 1 corresponding to intensity. B-D, Binary image at a threshold of $t = 1.0$, 0.5 and 0.0 respectively. E, The filtrations matrix constructed by assigning each pixel a value corresponding to the order at which it was activated. Pixels which became active at the same threshold are numbered arbitrarily. F-H, The corresponding network representation of the image at filtration values corresponding to the thresholds above. Here, f denotes the maximum filtration value permitted. As the filtration value increases, two connected components form and then merge into one object. I, The persistence diagram constructed from the topological decomposition of the image. This plots the birth threshold, b, against the death threshold, d, for each object identified. The persistence of each object is represented by $\tau = b - d$. Two prominent points are found in region Y, given by $\tau \geq 0.5$, which correspond to the two bright objects in the original image

Each image was 256 by 256 pixels in size, with each pixel's brightness intensity defined between 0 and 1. Prominent objects were defined at the maximum intensity of 1 over a background defined at 0 for images a-d and at varying intensities between 0.2 and 1 over a gradient background between 0 and 0.2 for images e-f. Further manipulation of each image was performed in RStudio. Gaussian noise (with standard deviations $\sigma_1 = 0, 0.5, 1$) was applied manually in R and Gaussian blur (with standard deviations $\sigma_2 = 0, 5, 10$) was applied using the blur function of the EBImage R package [18]. All images were subsequently normalised to return intensity values to the range of 0-1.

3 | RESULTS

3.1 | Description of the algorithm

TOBLERONE is initialised with two inputs: the matrix representation of a grayscale image, where each pixel represents an intensity value between 0 and 1, and a parameter known as the *persistence threshold*, which dictates the permitted range of differences in intensity between pixels corresponding to the same object. Given

that the image size and range of possible intensity values is finite, it is possible to produce a sequence of binarized images by thresholding over all possible intensities (Figure 1A-D). In order to undertake topological data analysis, each of these binary images must be ascribed an algebraic construct known as a simplicial complex. This is typically depicted in 2D space by a set of nodes (0-cells), connected by edges (1-cells) and spaces between three adjacent edges filled by a face (2-cells), giving the complex the appearance of a triangulation. To achieve this, TOBLERONE first maps each active pixel onto a node (or vertex) and assigns two nodes to be connected by an edge if they are immediately adjacent and are both active in the binary image—this representation is often referred to as the grid topology. The implementation of the grid topology (as the primary representation of an image) underpins the assumption that continuous objects are defined by a set of pixels in which a path between any two pixels can be achieved by a finite series of lateral or diagonal movements across pixels within the set.

As we progress sequentially through the series of binary images (Figure 1B-D), the number of nodes, edges and faces within the graphical representation of the simplicial complex increases. As such, we can assign each cell complex an ordered numerical value corresponding

to the stage of the binarization sequence at which it was first activated (Figure 1E). Mathematically, this is known as a filtration scheme, and each stage of the filtration will correspond to a different simplicial complex (Figure 1F-H) [19, 20]. While the definition of a topological feature typically incorporates holes in the complex, we restrict our usage here to the first homology class, which represents the number of distinct connected components [21–23]. Since the activation of an edge is imposed directly by the activation of the two nodes it is formed between, it suffices to observe the activation of pixels alone. Here, it is assumed that each identified connected component corresponds to a distinct biological structure.

By considering the image as a discretised representation of a continuous intensity field, we can identify the most prominent (ie, brightest) pixels as estimations of the local maxima within that field. These maxima are known as modes, and are typically among the first nodes to appear within the filtration. As the filtration progresses, more nodes will be activated within the vicinity of the original mode and become connected. Since the mode is inherently defined as a local maximum, each newly added node will have a filtration value higher than that of the original. This induces a discretised gradient vector field upon the simplicial complex corresponding to the differences in filtration values between neighbouring nodes. To each mode, we can then assign a region corresponding to the set of nodes which are connected to the given mode [13]. Neighbouring regions are merged to form a single connected component with the new mode defined to be the younger of the two original modes, that is, the pixel with the lowest filtration value. This process is known as mode-seeking and it is the principle which allows each connected component to be identified.

At the end of the filtration, only one mode will remain. This corresponds to the pixel with highest intensity value, and it will be connected to all pixels in the image. This means that, throughout the process of generating the filtration, each mode is formed and then subsequently destroyed, save for the final mode which will not be a good representation of the segmentation. As such, each root has an associated birth scale, the threshold at which the root and its corresponding connected component is created, and death scale, the threshold at which the region of interest intersects another and is absorbed. The difference between the birth and death scale is known as the *persistence*. This can be recorded for each connected component identified and represented via a persistence diagram (Figure 1i), which plots the birth scale against the death scale for each region [24]. Each point on this diagram corresponds to a connected component. We are particularly interested in those which have high birth scales and low death scales, as these

correspond to regions of the space which form at high thresholds and do not merge with the background until particularly low thresholds are reached. By selecting an appropriate persistence threshold, we can extract only the most persistent connected components. In a biological setting, this allows for identification and extraction of structures visible within the image, and essentially segments each object. After each implementation, TOBLERONE will return the number of connected components found with the given persistence threshold.

An appropriate persistence threshold can be ascertained iteratively by arbitrarily initialising at $\tau = 0.5$ and perturbing the threshold to match the expected number of connected components (in this context, the expected number of cells). Increasing the threshold will yield greater merging and reduce the number of connected components found, while decreasing the threshold will promote more pronounced segmentation and increase the number of connected components found. As a topological data analysis technique, TOBLERONE is stable with respect to perturbations in persistence. As such, small changes to the choice of the persistence threshold will not impact the number of objects or their boundaries. Unless changing the persistence impacts the number of objects found, the change of parameter will have little effect on the boundaries returned, so finetuning is not required. In the context of cell segmentation across multiple images, the recommended method for estimating an appropriate persistence is to take a representative image, determine how many cells or clusters of cells are present, and alter the input persistence as described above until that number is returned. Provided all other images were acquired under the same microscope conditions, the same persistence threshold can be applied to all images in the data set.

Once the segmentation has been finalised, the algorithm will extract the exterior boundary of each object. However, probing micro-heterogeneity in membrane properties requires an additional understanding of the orientation of the circuit of pixels corresponding to the plasma membrane. As such, TOBLERONE employs a variation of the Swinging Arm method which preserves the ordering of each pixel comprising the boundary layer, initialised at the top-left-most pixel and proceeding counter-clockwise until returning to the origin [25]. This boundary can then be deleted from the image and the process can be repeated an arbitrary number of times, allowing the choice of layer selection at varying depths within the object. The choice of layer is based on user preference, depending on the region of the cell or membrane they wish to acquire. Indeed, provided the persistence threshold has been selected appropriately, the boundary of the objects found will correspond to the

FIGURE 2 A-F, A series of toy images exhibiting a range of geometries and topologies. Noise and blur are simulated over each image and then TOBLERONE, Otsu thresholding and the Watershed algorithm are performed to recover the original segmentation. Primary segmentations were identified using a persistence threshold of 0.5 for TOBLERONE and using the recommended settings for the Watershed algorithm
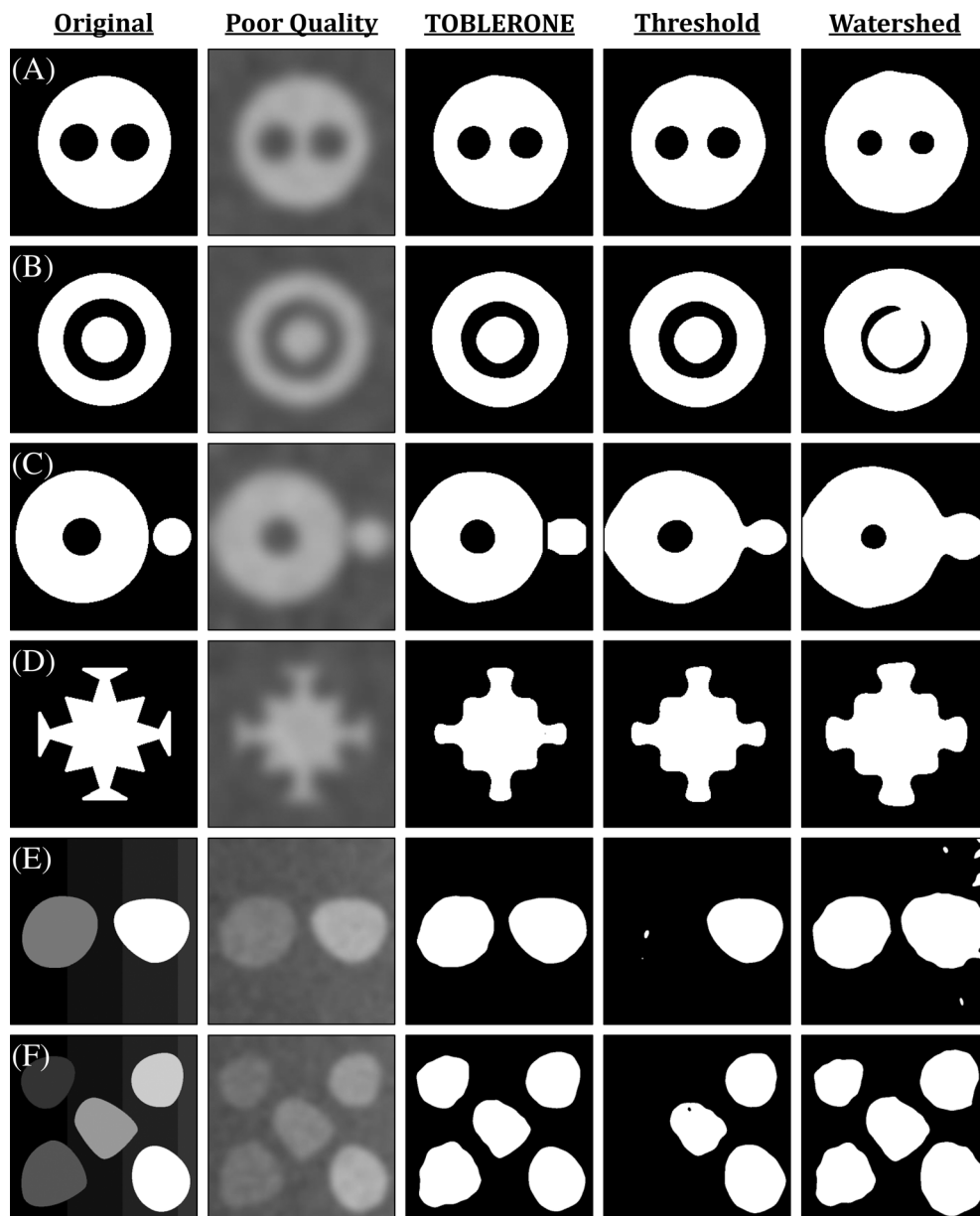
boundaries of the cells. With this in mind, selecting precisely one iteration of the Swinging Arm method will provide the exact exterior boundary. However, users may wish the increase the number of iterations in order to discriminate between the inner and outer leaflets of the membrane (say) or take a representative portion of the cytoplasm. The algorithmic process culminates in the output of a given cell segmentation and the oriented loops corresponding to the boundaries of each found object.

3.2 | Demonstration with simulated data

Using a series of simulated images, with highly varied geometries and topologies, we have found that TOBLERONE can identify and segment binary images with high

sensitivity and specificity (Figure 2A-F). First, binary objects were generated and Gaussian noise was simulated over each pixel in each image with standard deviation $\sigma_1 = 1$. Then, Gaussian blur was applied with standard deviation $\sigma_2 = 10$. These parameters were chosen to approximately recapitulate the image quality obtained from conventional confocal microscopy. Each image was segmented using TOBLERONE as well as two alternative segmentation approaches, Otsu's method and the Watershed algorithm, to compare against the performance of TOBLERONE [26, 27]. We then quantified each algorithm's sensitivity (fraction of ground-truth foreground pixels correctly labelled as active by the algorithm) and specificity (fraction of ground-truth background pixels correctly labelled as inactive). To avoid skewing sensitivity and specificity, we only considered pixels within an 11 by

Image ID	TOBLERONE			Otsu thresholding			Watershed		
	Sens	Spec	#	Sens	Spec	#	Sens	Spec	#
a	0.992	0.904	Y	0.995	0.900	Y	1.000	0.090	Y
b	0.983	0.848	Y	0.992	0.789	Y	1.000	0.085	N
c	0.896	0.911	Y	0.955	0.809	N	1.000	0.113	N
d	0.773	0.749		0.822	0.673	Y	0.953	0.312	Y
e	0.926	0.725	Y	0.482	0.949	N	0.972	0.394	N
f	0.685	0.894	Y	0.363	0.918	N	0.688	0.526	N

TABLE 1 Sensitivity (Sens) and specificity (Spec) of each algorithm on each simulated image under noise and blur, as seen in Figure 2

Note: If the correct number of connected components was found, the entry in the number column (#) was marked with Y, otherwise it was marked with N.
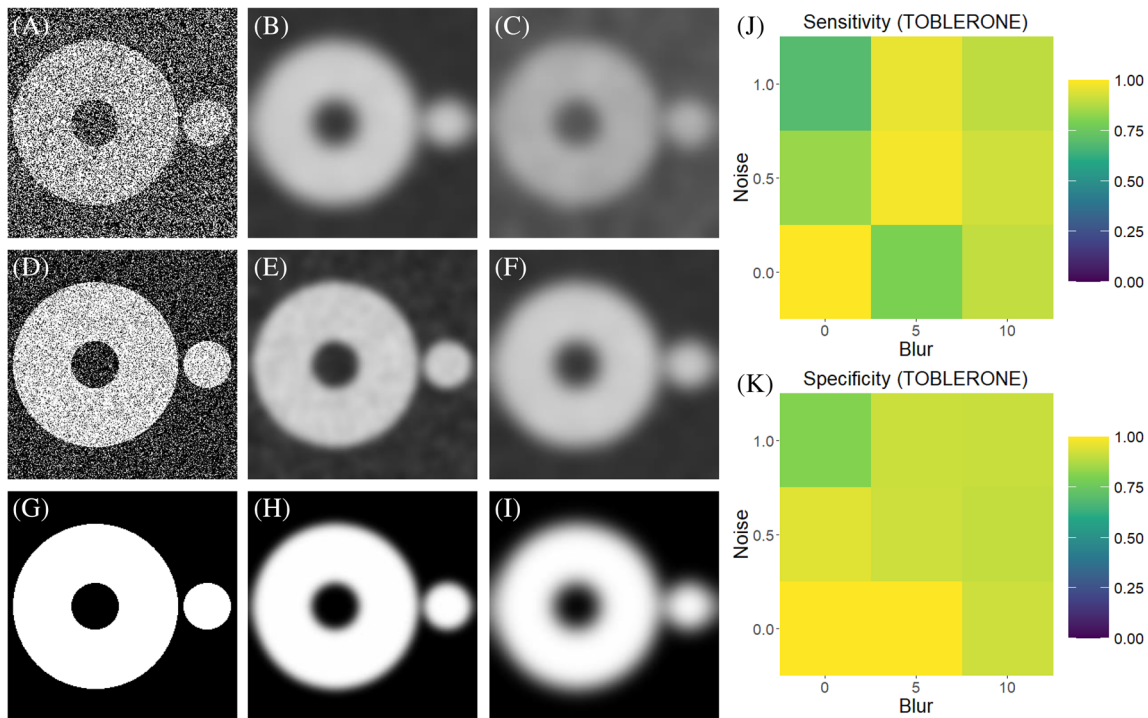

FIGURE 3 A-I, A simulated image of two different objects with varying degrees of noise and blur applied. J-K, Heatmaps of the sensitivity and specificity (as defined above) of TOBLERONE on each of the corresponding images A-I. While there is little variation observed in either value, results suggest that noise has a greater negative impact on the algorithm's performance

11 grid around each pixel comprising the object's boundary (5 pixels in each direction). Additionally, we recorded the number of connected components found by each algorithm. Notably, only TOBLERONE consistently returned the correct number of connected components.

Under these conditions, TOBLERONE achieved a sensitivity of 0.8765 and a specificity of 0.8762 (averaged over the six simulated image conditions)—this means that almost all pixels belonging to an object were correctly identified and most pixels belonging to the background were correctly ignored, respectively. Both statistics surpassed their counterparts for Otsu thresholding (0.7686 and 0.8402 respectively) and TOBLERONE's specificity was far greater than that of watershed algorithm (0.2533).

In this case, the sensitivity of the watershed algorithm (0.9355) was greater only on account of oversaturation of the segmentations. Summary data is given in entirety in Table 1 and suggests that TOBLERONE is capable of accurately and precisely segmenting objects, even under poor image quality, and outperforms existing non-machine learning-based segmentation methods.

To further probe the impact of noise and blur on TOBLERONE's performance, we extracted one image from the simulation data set and applied varying degrees of noise and blur. Each image was segmented by the algorithm and sensitivity and specificity were recalculated. Results are given in Figure 3 and show that TOBLERONE yields a small drop in both sensitivity and
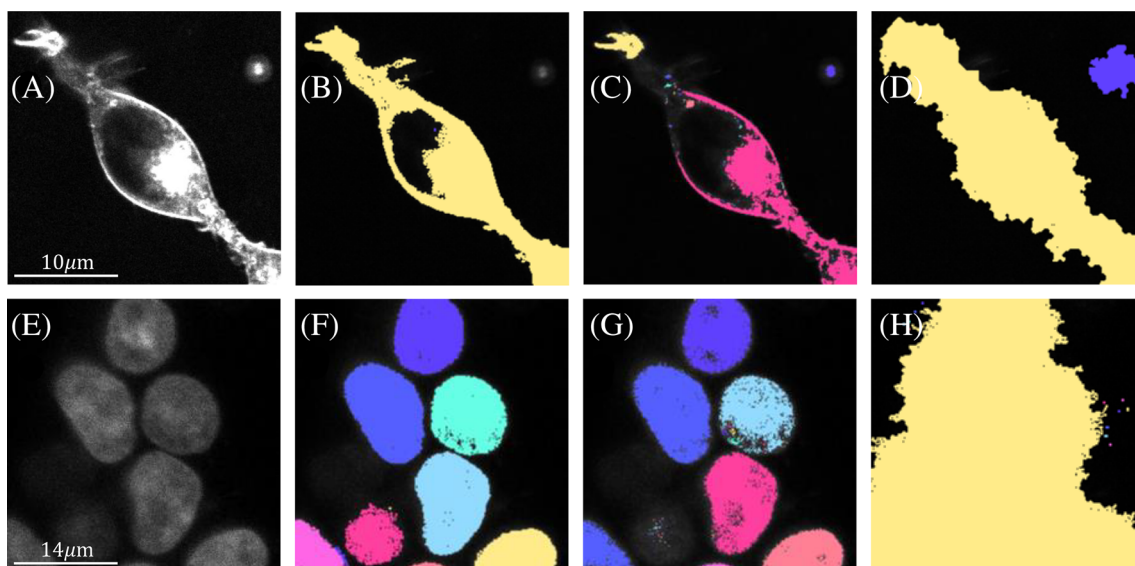
FIGURE 4 A, Image of a HEK293 cell stained with di-4-ANEPPDHQ. B-D, Masks of the HEK cell as identified by TOBLERONE, Otsu thresholding and the Watershed algorithm, respectively. Protrusions and variations in membrane morphology are captured by TOBLERONE despite the heterogeneous geometry. E, An image of several HEK cell nuclei stained with Nucblue. F-H, Masks of each nucleus as identified by TOBLERONE, Otsu thresholding and the Watershed method, respectively

specificity as either noise or blur are increased. Notably, applying a simple denoising technique, such as blurring, seems to improve both the sensitivity and specificity of the algorithm.

3.3 | Demonstration with experimental data

We then used TOBLERONE to assess two cell types: the R265 strain of *C gattii*, which typically exhibits an approximately spherical geometry, and human embryonic kidney (HEK) cells, which display a more complex morphology incorporating finger-like protrusions. HEK Cells were cultured in DMEM media and cryptococcal cells in YPD media in coverslip-bottomed microscope dishes, stained with di-4-ANEPPDHQ (membranes) or Nucblue (DNA) for 20 minutes at 37°C and imaged live via confocal microscopy. Segmentation was undertaken using TOBLERONE, Otsu thresholding and the Watershed algorithm, with examples displayed in Figure 4. Of the three algorithms considered, TOBLERONE is the only method to successfully identify the highly non-convex morphologies of the HEK cells and shows the greatest discrimination against the background. Results suggest that both HEK cells (Figure 4A-D) and their nuclei (Figure 4E-H) can be identified using TOBLERONE.

C gattii is an infectious species of fungus which is responsible for cryptococcal meningitis in humans.

TOBLERONE was used to identify the membranes of these cells (Figure 5). The degree of membrane order, represented by the Generalised Polarisation (GP) images (Figure 5A-C), was calculated. The GP line profiles (Figure 5G) were then extracted from the boundaries of the masks (Figure 5D-F). The average GP was extracted for control cells as well as those treated with 2-hydroxyoleic acid or 7-ketocholesterol, which are predicted to introduce a higher degree of membrane disorder (Figure 5H). A statistically significant difference in the mean GP value was identified at the significance level of 1%, suggesting that both 2OHOA and 7-ketocholesterol reduce membrane order in *C gattii*.

4 | DISCUSSION

In this work, we introduce TOBLERONE, an image segmentation algorithm specifically designed for identifying cells and organelles in fluorescence microscopy images, which operates without the drawbacks of conventional geometric and machine learning-based image segmentation methods. We have explored the mathematical principles which underpin the functionality of TOBLERONE, namely, in the use of topological data analysis for extracting the homology classes of the image under different thresholds. We then applied the algorithm to a range of simulated images—achieving high sensitivity and specificity even under particularly poor image quality—and a selection of differing cell and organelle geometries,
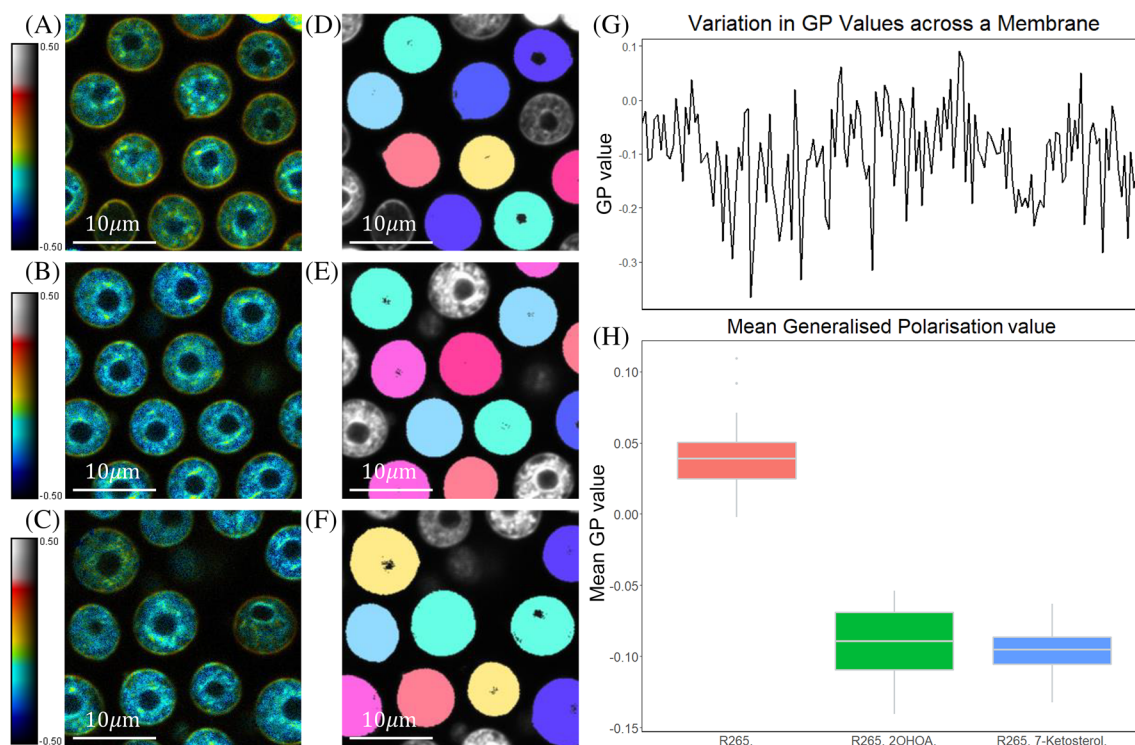
FIGURE 5 A-C, GP images of *C gattii* cells from the control group, those treated with 2OHOA and those treated with 7-ketocholesterol, respectively. Cells were stained with di-4-ANEPPDHQ. Pseudocolour applied to reflect the difference in GP values across the membrane. D-F, Masks of the same cells, as found by TOBLERONE, overlaid onto the grayscale images. Dead and incomplete cells lying on the periphery have been manually excluded. G, The GP line profile extracted from the boundary of an arbitrary cell. H, Boxplot depicting the average GP value across the membrane for cells treated with 2OHOA or 7-ketocholesterol

including variants of the R265 strain of *C gattii*, as well as HEK cells and their nuclei. We showed that TOBLERONE outperforms existing segmentation methods by achieving higher sensitivity and specificity under varying degrees of noise and blur. Additionally, we have highlighted the qualitative benefits of TOBLERONE over traditional geometric segmentation algorithms when applied to real experimental data. This demonstrated the applicability of TOBLERONE in practice by objectively identifying structures, biological or otherwise, of arbitrary shape. By exploiting topological properties of the boundaries of these structures, we were able to identify the plasma membrane of *C gattii* and produce quantitative analysis of membrane order.

In comparison to the existing methods for image segmentation, TOBLERONE does present the following drawbacks. It is currently limited to 2D images, and its performance will be dependent on image quality [28]. Computationally, the primary segmentation's runtime is on-par with existing machine learning methods, but pre-processing and boundary identification often take longer [6, 9]. While TOBLERONE can function with only a single parameter, it is not always obvious how to appropriately select its value—however, topological features in

images are typically robust to variations in intensity, so a range of persistence thresholds will usually return a suitable segmentation [29–31]. As a topological image analysis technique, TOBLERONE is invariant of cell and organelle morphology [32, 33]. While this makes the algorithm highly generalisable, it can present challenges in dense cell lines, as the algorithm may merge cells in close proximity, particularly when there is no visible gap between them.

The advantages of TOBLERONE over the general geometry-based approaches are as follows. TOBLERONE presents the advantage that it can segment structures of any size and shape, provided they are well-separated from surrounding objects and the background. In microscopy, this alleviates the need for pre-existing knowledge of the geometric properties of cells and, in the case of machine learning, training data sets of any kind. Not only does this counteract over-parameterisation, but it reduces the impact of parameter estimation. Additionally, since TOBLERONE is invariant of geometric cell properties, it is applicable even to images with a high degree of between-cell variation. As such, topological image analysis is best employed when the images contain structures of varied or complex geometry—particularly those with

highly non-convex structures. Typically, it is more likely that geometric techniques would outperform topological methods in instances where cells form dense, connected tissues.

Generally, TOBLERONE probes images containing structures of any topology, including those which appear to present gaps within the structures themselves. This principle allows for the identification of both exterior boundaries, corresponding to the cell membrane, and interior boundaries, which may correspond to organelles, vesicles or other structures contained within the cells. As TOBLERONE is a topological methodology, it is able to distinguish between the different boundary types automatically. Overall, this tool presents a different approach to image analysis compared to geometrical or machine-learning based image segmentation with considerable advantages for identifying cell boundaries.

CONFLICTS OF INTEREST
The authors declare no financial or commercial conflict of interest.

DATA AVAILABILITY STATEMENT
Images used in this study are available at https://github.com/lucapanconi/toblerone. The data that support the findings of this study are available from the corresponding author upon reasonable request.

AUTHOR BIOGRAPHIES
Please see Supporting Information online.

ORCID
Luca Panconi https://orcid.org/0000-0001-6025-8597

REFERENCES
[1] T. Vicar, J. Balvan, J. Jaros, F. Jug, R. Kolar, M. Masarik, J. Gumulec BMC Bioinform. **2019**, *20*, 360.
[2] J. Chalfoun, M. Majurski, A. Dima, C. Stuelten, A. Peskin, M. Brady, BMC Bioinform. **2014**, *15*, 431.
[3] S. Raman, C. A. Maxwell, M. H. Barcellos-Hoff, B. Parvin, J. Microsc. **2007**, *225*, 22.
[4] T. Scherr, K. Löffler, M. Böhland, R. Mikut, PLoS One **2020**, *15*, e0243219.
[5] J. Stegmaier, J. C. Otte, A. Kobitski, A. Bartschat, A. Garcia, G. U. Nienhaus, U. Strähle, R. Mikut, PLoS One **2014**, *9*, e90036.
[6] C. Stringer, T. Wang, M. Michaelos, M. Pachitariu, Nat. Methods **2021**, *18*, 100.
[7] Y. Al-Kofahi, A. Zaltsman, R. Graves, W. Marshall, M. Rusu, BMC Bioinform. **2018**, *19*, 365.
[8] Y. Jin, A. Toberoff, E. Azizi, bioRxiv **2021**.
[9] U. Schmidt, M. Weigert, C. Broaddus, G. Myers, *Cell Detection with Star-Convex Polygons*, Springer International Publishing, Cham **2018**.
[10] P. Edwards, K. Skruber, N. Milićević, J. B. Heidings, T.-A. Read, P. Bubenik, E. A. Vitriol, Patterns. **2021**, *2*, 11.
[11] R. Rojas-Moraleda, W. Xiong, N. Halama, K. Breitkopf-Heinlein, S. Dooley, L. Salinas, D. W. Heermann, N. A. Valous, Med. Image Anal. **2017**, *38*, 90.
[12] N. Otter, M. A. Porter, U. Tillmann, P. Grindrod, H. A. Harrington, EPJ Data Science **2017**, *6*, 17.
[13] F. Chazal, L. Guibas, S. Oudot, P. Skraba, J ACM **2011**, *60*, 1.
[14] E. Sezgin, T. Gutmann, T. Buhl, R. Dirkx, M. Grzybek, Ü. Coskun, M. Solimena, K. Simons, I. Levental, P. Schwille, PLoS One **2015**, *10*, e0123930.
[15] D. M. Owen, C. Rentero, A. Magenau, A. Abu-Siniyeh, K. Gaus, Nat. Protoc. **2011**, *7*, 24.
[16] D. M. Owen, D. Williamson, C. Rentero, K. Gaus, Traffic **2009**, *10*, 962.
[17] T. Parasassi, G. De Stasio, A. d'Ubaldo, E. Gratton, Biophys. J. **1990**, *57*, 1179.
[18] G. Pau, F. Fuchs, O. Sklyar, M. Boutros, W. Huber, Bioinformatics **2010**, *26*, 979.
[19] N. Byrne, J. R. Clough, I. Valverde, G. Montana, A. P. King, IEEE T. Parts. Anal. **2021**, *1*, 1.
[20] R. Assaf, A. Goupil, V. Vrabie, T. Boudier, M. Kacim, Pattern Recog. Lett. **2018**, *112*, 277.
[21] R. Assaf, A. Goupil, M. Kacim, V. Vrabie, *Topological Persistence Based on Pixels for Object Segmentation in Biomedical Images*, IEEE, New York **2017**.
[22] J. Clough, I. Oksuz, N. Byrne, J. Schnabel, A. King, Springer, **2019**, *11492*, 16.
[23] Y.-M. Chung, C.-S. Hu, A. Lawson, C. Smyth, IEEE International Conference on Big Data (Big Data), **2018**, 100–105.
[24] O. Vipond, A. Bull Joshua, S. Macklin Philip, U. Tillmann, W. Pugh Christopher, M. Byrne Helen, A. Harrington Heather, Proc. Natl. Acad. Sci. **2021**, *118* e2102166118.
[25] A. Galton, M. Duckham, *What Is the Region Occupied by a Set of Points?*, Springer, New York **2006**.
[26] K. V. Lalitha, R. Amrutha, S. Michahial, M. Shivakumar, IJARCCE **2016**, *5*, 196.
[27] N. Otsu, IEEE Trans. Syst. Man Cybern. **1979**, *9*, 62.
[28] G. V. Pednekar, J. K. Udupa, D. J. McLaughlin, X. Wu, Y. Tong, C. B. Simone 2nd., J. Camaratta, D. A. Torigian, Proc. SPIE Int. Soc. Opt. Eng. **2018**, *85*, 10576.
[29] H. Masoomy, B. Askari, M. N. Najafi, S. M. S. Movahed, Phys. Rev. E **2021**, *104*, 034116.
[30] R. Turkeš, J. Nys, T. Verdonck, S. Latré, PLoS One **2021**, *16*, e0257215.
[31] N. Atienza, R. Gonzalez-Díaz, M. Rucco, Springer, New York **2016**.
[32] F. Chazal, B. Michel, Front. Artif. Intell. **2021**, *29*, 4.

[33] A. Alatorre, J. M. Casillas, F. Becerra López, *J. Adv. Res.* **2018**, *2*, 1.

SUPPORTING INFORMATION

Additional supporting information can be found online in the Supporting Information section at the end of this article.